DOI: 10.3901/CJME.2016.0122.012, available online at www.springerlink.com; www.cjmenet.com

Method for Six-Legged Robot Stepping on Obstacles by Indirect Force Estimation

XU Yilin, GAO Feng*, PAN Yang, and CHAI Xun

State Key Laboratory of Mechanical System and Vibration, Shanghai Jiao Tong University, Shanghai 200240, China

Received May 13, 2015; revised January 20, 2016; accepted January 22, 2016

Abstract: Adaptive gaits for legged robots often requires force sensors installed on foot-tips, however impact, temperature or humidity can affect or even damage those sensors. Efforts have been made to realize indirect force estimation on the legged robots using leg structures based on planar mechanisms. Robot Octopus III is a six-legged robot using spatial parallel mechanism(UP-2UPS) legs. This paper proposed a novel method to realize indirect force estimation on walking robot based on a spatial parallel mechanism. The direct kinematics model and the inverse kinematics model are established. The force Jacobian matrix is derived based on the kinematics model. Thus, the indirect force estimation model is established. Then, the relation between the output torques of the three motors installed on one leg to the external force exerted on the foot tip is described. Furthermore, an adaptive tripod static gait is designed. The robot alters its leg trajectory to step on obstacles by using the proposed adaptive gait. Both the indirect force estimation model and the adaptive gait are implemented and optimized in a real time control system. An experiment is carried out to validate the indirect force estimation model. The adaptive gait is tested in another experiment. Experiment results show that the robot can successfully step on a 0.2 m-high obstacle. This paper proposes a novel method to overcome obstacles for the six-legged robot using spatial parallel mechanism legs and to avoid installing the electric force sensors in harsh environment of the robot's foot tips.

Keywords: robot, parallel mechanism, force estimation, obstacle

1 Introduction

Legged locomotion is a common locomotion form in the nature world. Many robotics researchers have been inspired by animals. Thus researches of the legged robots have become an important portion of robotics. Theoretically speaking, comparing with wheeled robots or tracked robots, legged robots have better mobility over rough terrain.

Basically, when a robot negotiates with the environment, information about the environment needs to be gathered. This means that various kinds of sensors should be installed on the robot. For contact and obstacle detection, force sensor is a common device in such application. In many robot systems, force sensors are essential devices[1–6]. COMET-I[3] is a six-legged robot designed to detect mine. On its foot tip, metal sensor, optical proximity sensor and force sensor are installed. This robot uses hybrid control including position and force control to realize stable walking on rough terrain. BigDog[4] is a quadruped robot developed by Boston Dynamics. There are about 50 sensors installed on this robot, including force sensors on its foot tip. With these components, the robot can adjust ground interaction forces.

Unfortunately, more sensors give rise to more costs and complexity. Usually, a force sensor or load cell is an expensive and delicate electronic device, which means that the tough environment near the contact point becomes a problem. The electronic device may be affected or even damaged by the temperature, humidity, collision, etc. From a control perspective, a stiff load cell causes stability problem under a high-gain feedback controller, which has a better response[7]. For these reasons, robot researchers, no matter focusing on legged robots or manipulators, have put many efforts to find alternative ways to detect collisions or measure the external forces.

These efforts resulted in various methods that realize the function of a force sensor in some degree. Serial elastic actuators[7] replace the load cell with a compliant elastic element. The deflection is measured by a position sensor, and the force is estimated based on Hooke's law. Comparing to hydraulic actuation or highly geared motors, these actuators have lower impedance. High fidelity force control is realized on the series elastic actuators. Other manipulator researchers introduce different force estimation methods base on the motor torque and standard proprioceptive sensors. FDI(fault detection and isolation) technique is used to calculate a residual vector which represents the joint torques producing from Cartesian contact forces[8]. This method uses joint encoders and motor command torques instead of force sensors. Also the

* Corresponding author. E-mail: fengg@sjtu.edu.cn
Supported by National Basic Research Program of China(973 Program, Grant No. 2013CB035501), and Research Fund of the State Key Lab of MSV of China(Grant No.MSV201208)

robot dynamics model is required. It can detect the collision that occurs at any point along the robot arm. Methods based on disturbance observer or reaction torque observer[9–10] also require robot dynamics model and take the joint position and the motor current as inputs of the force estimation method.

For legged robots, there are also many different attempts to achieve indirect force estimation. For the biped robot NAO, BELLACCINI, et al[11], developed an equilibrium interaction technique that does not require force sensors. The method using IMU to measure the position and the velocity of the center of the mass, and the position and the velocity of the center of the mass determine the instantaneous capture point. Then the external force by the perturbation of the instantaneous capture point can be calculated. Then the robot can react to the external force. Another way to solve this question is based on the fact that when the force is applied on the robot, small deviation or deformation on its structure occurs. The parallel link walking robot ParaWalker-S1[12] uses potentiometer to measure the small deviation of the joint angle. Then the entire leg-drive mechanism acts as a 6-axis force sensor. With this peculiar structure, Smooth contact with the ground by the swing-leg is realized. Other robots use strain gauge on the certain location of the leg structure. Six-legged robot MYRMEX[13] uses strain gauges on the upper part of the leg. For hydraulic actuated robots, force estimation methods based on cylinder pressure are discussed. TIAN, et al[14], used pressure sensors and proprioceptive sensors to achieve indirect external disturbance force estimation. In the experiment, the robot Baby-Elephant uses the method to recognize changes in additional weight during the crawling gait walking. Pressure transducers are installed on the quadruped robot ROBOCLIMBER's double-effect hydraulic actuators[15]. The research of ROBOCLIMBER suggests that accurate, reliable, simplicity and low cost indirect force estimation can be achieved through careful studies of the hydraulic system behavior. For systems actuated by electric motors, the motor current becomes a reference of the collision or the external force. LAURON III[16] is a six-legged robot that employs coordinates force and current sensors to detect leg collisions during the transfer phase of each leg. The six-legged robot ARMU5 is based on the pantgraph mechanism. Its leg has 3 DOFs. Knowing the relationship between the motor output torque and the current through the motor, the current of the motor can be used to calculate the actual joint torque. The ideal dynamics model of the robot is established to calculate the ideal joint torque of the robot. The differences between the actual torque and the ideal torque will reveal if the robot foot contacts with the obstacle and the ground[17–18]. The MIT Cheetah robot is designed to be a highly efficient quadruped[19]. Researchers carefully design its actuator and leg structure. As a result, the robot has low inertia composite legs, dual coaxial actuator unit, low gear ratio and single stage gears. Thus the impact force applied on the foot during high speed locomotion can be estimated in high resolution[20].

In this study, focusing on a six-legged robot with parallel mechanism legs, a new method to step on the obstacle by indirect force estimation is implemented. The robot uses an adaptive tripod gait to step on the obstacle.

This paper is organized as follows. In section 2, the robot Octopus III is described. This study is based on this robot. In section 3, a force estimation model is established. With this model, the motor current is mapped to the foot tip force. The algorithm to generate adaptive trajectories is described in section 4. Two experiments are carried out on the six-legged robot Octopus III. In section 5, these experiments are described and the experiment data are analyzed. Finally, in section 6, there are some discussions on the current state and potential future works of the proposed method.

2 Robot Octopus III

Parallel manipulators have been an interesting research field for a long time[21–23]. But for six-legged robot, this kind of mechanism has not been widely used. This study is based on a robot with parallel mechanism legs. Octopus III(see Fig. 1) is a six-legged robot designed for carrying heavy load through uneven terrain. This robot is designed based on the robot Octopus II[24–25].

Fig. 1. Robot Octopus III

The new design changed the configuration of the legs and enhanced the designed walking speed. Its six legs have identical mechanism and are arranged symmetrically along the sagittal plane. For each leg, a 3 DOF spatial parallel mechanism(TriVariant[26]) is applied. This mechanism has three limbs. Two of them are UPS limbs. The UPS limb has a universal joint, a prismatic joint and a spherical joint connected in series from the body to the foot. The rest is a UP limb, which only has a universal joint and a prismatic joint connected in series.

The structure of whole system is illustrated by Fig. 2. A remote computer running Windows operation system is used for remote control. The robot has a control computer independently. These two computers connect each other through wireless network. There is a GUI program running

on the remote computer.

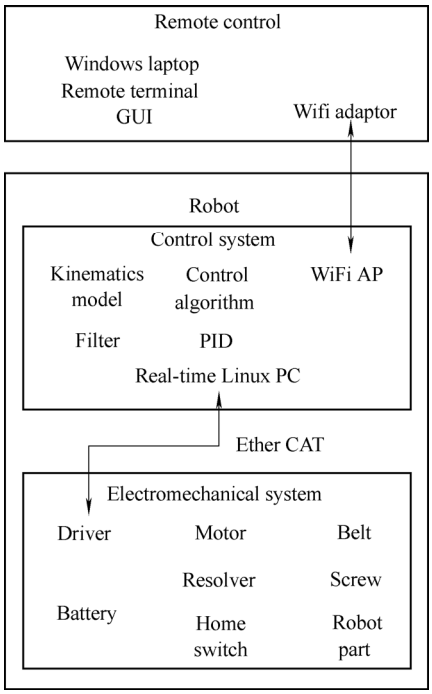

Fig. 2. Robot system structure

Orders like moving forward, turning left can be sent to the robot through this GUI program. The control computer has a 2249 MHz quad-core x86-64 CPU. The operation system is a Linux system with a patched kernel for real-time control. With the help of the real-time operation system, special optimized kinematics and dynamics models of the robot can be computed at a speed fulfilling the real-time control demand. The real-time control loop runs at 1000 Hz. In this paper, the real-time control program includes the PID algorithm, data filter, the direct kinematics model, the inverse direct model, the force estimation model and the algorithm of the adaptive gait. At the same frequency, the control computer exchanges data and command with the drives on the robot through EtherCAT real-time industrial fieldbus. The robot's motion is actuated by 18 motors, each of which is a 400 W power servo motor. The motors are carefully installed in the upper side of the leg. This structure is designed to make sure there is no electric device near the foot, which is easy to break under the hazard environment. The power is supplied by five lithium batteries. Servo motors, drivers and home switches are connected to the four of the batteries. The rest battery supplies power to the control computer.

Most parts of the robot are made of aluminum. Whole mass of the robot is about 270 kg. It can climb a 20° slope in the tripod gait. The maximal walking speed in the current optimized offline tripod gait is 1.08 km/h.

3 Indirect Force Estimation

The leg mechanism of the robot Octopus III is designed to avoid installing any electric devices near the foot. Under this circumstance, it is sensible to implement the indirect force estimation on the robot. The main idea of the indirect force estimation in this paper is establishing a mapping between the motor output torque and the foot tip contact force. Establishing the mapping needs to define a coordinate system on the robot at first. Then, the direct kinematics model and the inverse kinematics model are described. Finally, the mapping is described by a force Jacobian matrix.

3.1 Coordinate frames

First thing of establishing a kinematics model is defining necessary coordinate frames on the robot and the environment. The body coordinate frame and the global coordinate frame is illustrated in Fig. 3. The coordinate frames attached to the leg and the ankle are illustrated in Fig. 4.

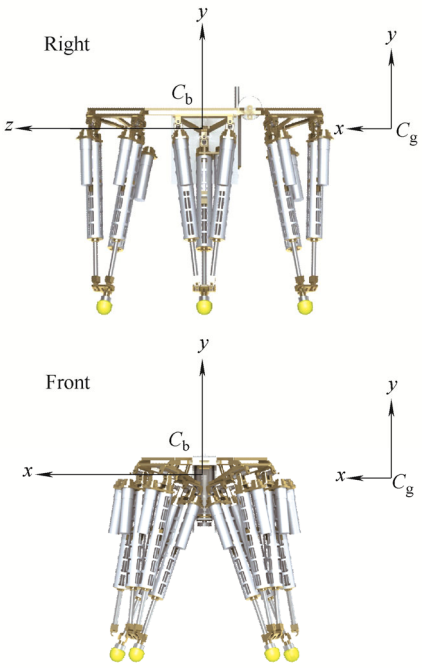

Fig. 3. Coordinate frames attached to the robot and the ground

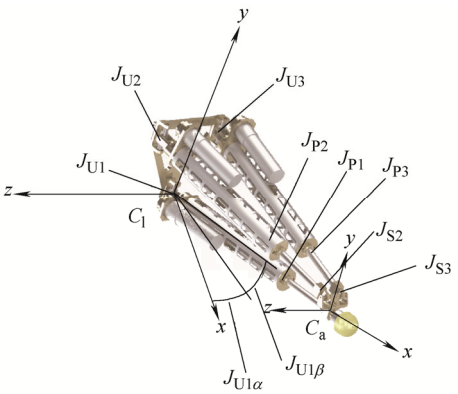

Fig. 4. Coordinate frames related to the robot leg

In Fig. 3, C_g represents the global coordinate frame, while C_b represents the body coordinate frame that is

attached to the robot body. In the body coordinate frame, the sagittal plane is the *y*-*z* plane. The transverse plane is the *x*-*z* plane. The coronal plane is the *x*-*y* plane. The relationship between the global coordinate frame and the body coordinate frame is arbitrary, since currently there is no IMU installed on the robot. For simplification, here we can define negative *y* direction of the global coordinate frame as the gravity direction. The initial posture is that each axis in body coordinate frame is parallel to the corresponding axis in the global coordinate frame. The distance between two origins can be any value convenient for the gait plan.

In Fig. 4, coordinate frames attached to one leg is illustrated. As all legs are identical in terms of their mechanism, each leg has the same coordinate system. In one leg, different subscript is used to distinguish different limb. For example, $\boldsymbol{J}_{\mathrm{U1}}$, $\boldsymbol{J}_{\mathrm{P1}}$ are joints in the UP limb. The subscript U represents the universal joint. The subscript P represents the prismatic joint. The subscript S represents the spherical joint. The leg coordinate frame C_{l} is fixed at the body. The origin of C_{l} is fixed at the intersection point of two rotation axis in the universal joint $\boldsymbol{J}_{\mathrm{U1}}$. The three universal joint, $\boldsymbol{J}_{\mathrm{U1}}$, $\boldsymbol{J}_{\mathrm{U2}}$ and $\boldsymbol{J}_{\mathrm{U3}}$, form a plane. The *x*-axis of C_l is perpendicular to this plane. The *y*-axis of C_{l} is parallel to the first rotation axis of the universal joint in the UP limb.

In the ankle of the leg, there is another coordinate frame C_{a}. It is fixed on the ankle of the leg. The *x*-axis of C_{a} is parallel to the sliding direction of the prismatic joint in the UP limb. When all the prismatic joints are at their shortest position, the corresponding axes of the coordinate frame C_{l} and C_{a} are parallel to each other. There are still some other notations in the Fig. 3. Notation $J_{\mathrm{U1}\alpha}$ denotes the angular displacement of the first rotation axis of the universal joint $\boldsymbol{J}_{\mathrm{U1}}$. Notation $J_{\mathrm{U1}\beta}$ denotes the angular displacement of the second rotation axis of the universal joint $\boldsymbol{J}_{\mathrm{U1}}$.

3.2 Kinematics model

This section will describe the derivation of the direct kinematics model and the inverse kinematics model of the robot leg. The displacement of three prismatic joints is denoted as $\boldsymbol{J}_{\mathrm{P1l}}$, $\boldsymbol{J}_{\mathrm{P21}}$ and $\boldsymbol{J}_{\mathrm{P31}}$. The notation $\boldsymbol{J}_{\mathrm{P1l}}$ represents the distance between $\boldsymbol{J}_{\mathrm{U1}}$ and $\boldsymbol{P}_{\mathrm{f}}$. The notation $\boldsymbol{J}_{\mathrm{P1l}}$ $\boldsymbol{J}_{\mathrm{P1l}}$ represents the distance between $\boldsymbol{J}_{\mathrm{U2}}$ and $\boldsymbol{J}_{\mathrm{S2}}$. These variables are the inputs of the model. The foot tip positon is denoted as $\boldsymbol{P}_{\mathrm{f}}$. It is the output of the model. To establish the model, two angular displacement $\boldsymbol{J}_{\mathrm{U1}\alpha}$ and $\boldsymbol{J}_{\mathrm{U1}\beta}$ should be derived at first. Then the pose matrix ${}^{\mathrm{l}}\boldsymbol{T}_{\mathrm{a}}$ can be calculated by multiplying two rotation matrices and one translation matrix:

$$ {}^{\mathrm{l}}\boldsymbol{T}_{\mathrm{a}} = \boldsymbol{R}_{\mathrm{U1}\alpha} \times \boldsymbol{R}_{\mathrm{U1}\beta} \times \boldsymbol{T}_{\mathrm{P1l}}, \tag{1} $$

where $\boldsymbol{R}_{\mathrm{U1}\alpha}$ —Rotation matrix about *y*-axis of the leg coordinate frame C_l,

$\boldsymbol{R}_{\mathrm{U1}\beta}$ —Rotation matrix about *z*- axis of the leg coordinate frame C_{l},

$\boldsymbol{T}_{\mathrm{P1l}}$ —Translation matrix of prismatic joint $\boldsymbol{J}_{\mathrm{P1}}$.

Matrix ${}^{\mathrm{l}}\boldsymbol{T}_{\mathrm{a}}$ will determine the position of foot tip in the leg coordinate frame C_{l}.

In the leg coordinate frame C_{l},

$$ \begin{cases} J_{\mathrm{P21}}^2 = \left|\boldsymbol{J}_{\mathrm{S2}}^{\mathrm{l}} - \boldsymbol{J}_{\mathrm{U2}}^{\mathrm{l}}\right|^{\mathrm{T}} \times \left|\boldsymbol{J}_{\mathrm{S2}}^{\mathrm{l}} - \boldsymbol{J}_{\mathrm{U2}}^{\mathrm{l}}\right|, \\ J_{\mathrm{P31}}^2 = \left|\boldsymbol{J}_{\mathrm{S3}}^{\mathrm{l}} - \boldsymbol{J}_{\mathrm{U3}}^{\mathrm{l}}\right|^{\mathrm{T}} \times \left|\boldsymbol{J}_{\mathrm{S3}}^{\mathrm{l}} - \boldsymbol{J}_{\mathrm{U3}}^{\mathrm{l}}\right|. \end{cases} \tag{2} $$

Expand the above equations,

$$ \begin{cases} J_{\mathrm{P21}}^2 = {\boldsymbol{J}_{\mathrm{S2}}^{\mathrm{l}}}^{\mathrm{T}} \times \boldsymbol{J}_{\mathrm{S2}}^{\mathrm{l}} - 2{\boldsymbol{J}_{\mathrm{U2}}^{\mathrm{l}}}^{\mathrm{T}} \times \boldsymbol{J}_{\mathrm{S2}}^{\mathrm{l}} + {\boldsymbol{J}_{\mathrm{U2}}^{\mathrm{l}}}^{\mathrm{T}} \times \boldsymbol{J}_{\mathrm{U2}}^{\mathrm{l}}, \\ J_{\mathrm{P31}}^2 = {\boldsymbol{J}_{\mathrm{S3}}^{\mathrm{l}}}^{\mathrm{T}} \times \boldsymbol{J}_{\mathrm{S3}}^{\mathrm{l}} - 2{\boldsymbol{J}_{\mathrm{U3}}^{\mathrm{l}}}^{\mathrm{T}} \times \boldsymbol{J}_{\mathrm{S3}}^{\mathrm{l}} + {\boldsymbol{J}_{\mathrm{U3}}^{\mathrm{l}}}^{\mathrm{T}} \times \boldsymbol{J}_{\mathrm{U3}}^{\mathrm{l}}. \end{cases} \tag{3} $$

In the above equations,

$$ \begin{cases} {\boldsymbol{J}_{\mathrm{S2}}^{\mathrm{l}}}^{\mathrm{T}} \times \boldsymbol{J}_{\mathrm{S2}}^{\mathrm{l}} = \begin{pmatrix} J_{\mathrm{S2}x}^{\mathrm{a}} + J_{\mathrm{P1l}} & J_{\mathrm{S2}y}^{\mathrm{a}} & J_{\mathrm{S2}z}^{\mathrm{a}} & 1 \end{pmatrix} \begin{pmatrix} J_{\mathrm{S2}x}^{\mathrm{a}} + J_{\mathrm{P1l}} \\ J_{\mathrm{S2}y}^{\mathrm{a}} \\ J_{\mathrm{S2}z}^{\mathrm{a}} \\ 1 \end{pmatrix}, \\ {\boldsymbol{J}_{\mathrm{S3}}^{\mathrm{l}}}^{\mathrm{T}} \times \boldsymbol{J}_{\mathrm{S3}}^{\mathrm{l}} = \begin{pmatrix} J_{\mathrm{S3}x}^{\mathrm{a}} + J_{\mathrm{P1l}} & J_{\mathrm{S3}y}^{\mathrm{a}} & J_{\mathrm{S3}z}^{\mathrm{a}} & 1 \end{pmatrix} \begin{pmatrix} J_{\mathrm{S3}x}^{\mathrm{a}} + J_{\mathrm{P1l}} \\ J_{\mathrm{S3}y}^{\mathrm{a}} \\ J_{\mathrm{S3}z}^{\mathrm{a}} \\ 1 \end{pmatrix}, \end{cases} \tag{4} $$

$$ \begin{cases} {\boldsymbol{J}_{\mathrm{U2}}^{\mathrm{l}}}^{\mathrm{T}} \times \boldsymbol{J}_{\mathrm{S2}}^{\mathrm{l}} = \begin{pmatrix} J_{\mathrm{U2}x}^{\mathrm{l}} & J_{\mathrm{U2}y}^{\mathrm{l}} & J_{\mathrm{U2}z}^{\mathrm{l}} \end{pmatrix} \times \boldsymbol{M} \times \begin{pmatrix} J_{\mathrm{S2}x}^{\mathrm{a}} + J_{\mathrm{P1l}} \\ J_{\mathrm{S2}y}^{\mathrm{a}} \\ J_{\mathrm{S2}z}^{\mathrm{a}} \end{pmatrix} + 1, \\ {\boldsymbol{J}_{\mathrm{U3}}^{\mathrm{l}}}^{\mathrm{T}} \times \boldsymbol{J}_{\mathrm{S3}}^{\mathrm{l}} = \begin{pmatrix} J_{\mathrm{U3}x}^{\mathrm{l}} & J_{\mathrm{U3}y}^{\mathrm{l}} & J_{\mathrm{U3}z}^{\mathrm{l}} \end{pmatrix} \times \boldsymbol{M} \times \begin{pmatrix} J_{\mathrm{S3}x}^{\mathrm{a}} + J_{\mathrm{P1l}} \\ J_{\mathrm{S3}y}^{\mathrm{a}} \\ J_{\mathrm{S3}z}^{\mathrm{a}} \end{pmatrix} + 1. \end{cases} \tag{5} $$

Matrix $\boldsymbol{M}$ in the above equations is

$$ \boldsymbol{M} = \begin{pmatrix} \cos J_{\mathrm{U1}\alpha} \cos J_{\mathrm{U1}\beta} & -\cos J_{\mathrm{U1}\alpha} \cos J_{\mathrm{U1}\beta} & \sin J_{\mathrm{U1}\alpha} \\ \sin J_{\mathrm{U1}\alpha} & \cos J_{\mathrm{U1}\beta} & 0 \\ -\sin J_{\mathrm{U1}\alpha} \cos J_{\mathrm{U1}\beta} & \sin J_{\mathrm{U1}\alpha} \sin J_{\mathrm{U1}\beta} & \cos J_{\mathrm{U1}\alpha} \end{pmatrix}. \tag{6} $$

$$ \begin{cases} {\boldsymbol{J}_{\mathrm{U2}}^{\mathrm{l}}}^{\mathrm{T}} \bullet \boldsymbol{J}_{\mathrm{U2}}^{\mathrm{l}} = {\boldsymbol{J}_{\mathrm{U2}x}^{\mathrm{l}}}^2 + {\boldsymbol{J}_{\mathrm{U2}y}^{\mathrm{l}}}^2 + {\boldsymbol{J}_{\mathrm{U2}z}^{\mathrm{l}}}^2 + 1, \\ {\boldsymbol{J}_{\mathrm{U3}}^{\mathrm{l}}}^{\mathrm{T}} \bullet \boldsymbol{J}_{\mathrm{U3}}^{\mathrm{l}} = {\boldsymbol{J}_{\mathrm{U3}x}^{\mathrm{l}}}^2 + {\boldsymbol{J}_{\mathrm{U3}y}^{\mathrm{l}}}^2 + {\boldsymbol{J}_{\mathrm{U3}z}^{\mathrm{l}}}^2 + 1. \end{cases} \tag{7} $$

Rearranging these equations,

$$\begin{cases} 2\begin{pmatrix} \boldsymbol{J}^{\mathrm{l}}_{\mathrm{U}2x} & \boldsymbol{J}^{\mathrm{l}}_{\mathrm{U}2y} & \boldsymbol{J}^{\mathrm{l}}_{\mathrm{U}2z} \end{pmatrix} \times \boldsymbol{M} \times \begin{pmatrix} \boldsymbol{J}^{\mathrm{a}}_{\mathrm{S}2x} + \boldsymbol{J}_{\mathrm{P1l}} \\ \boldsymbol{J}^{\mathrm{a}}_{\mathrm{S}2y} \\ \boldsymbol{J}^{\mathrm{a}}_{\mathrm{S}2z} \end{pmatrix} = \\ (\boldsymbol{J}_{\mathrm{P1l}} + \boldsymbol{J}^{\mathrm{a}}_{\mathrm{S}2x})^2 + \boldsymbol{J}^{\mathrm{a}}_{\mathrm{S}2y}{}^2 + \boldsymbol{J}^{\mathrm{a}}_{\mathrm{S}2z}{}^2 + \boldsymbol{J}^{\mathrm{l}}_{\mathrm{U}2x}{}^2 + \\ \boldsymbol{J}^{\mathrm{l}}_{\mathrm{U}2y}{}^2 + \boldsymbol{J}^{\mathrm{l}}_{\mathrm{U}2z}{}^2 - \boldsymbol{J}_{\mathrm{P1l}}{}^2, \\ 2\begin{pmatrix} \boldsymbol{J}^{\mathrm{l}}_{\mathrm{U}3x} & \boldsymbol{J}^{\mathrm{l}}_{\mathrm{U}3y} & \boldsymbol{J}^{\mathrm{l}}_{\mathrm{U}3z} \end{pmatrix} \times \boldsymbol{M} \times \begin{pmatrix} \boldsymbol{J}^{\mathrm{a}}_{\mathrm{S}3x} + \boldsymbol{J}_{\mathrm{P1l}} \\ \boldsymbol{J}^{\mathrm{a}}_{\mathrm{S}3y} \\ \boldsymbol{J}^{\mathrm{a}}_{\mathrm{S}3z} \end{pmatrix} = \\ (\boldsymbol{J}_{\mathrm{P1l}} + \boldsymbol{J}^{\mathrm{a}}_{\mathrm{S}3x})^2 + \boldsymbol{J}^{\mathrm{a}}_{\mathrm{S}3y}{}^2 + \boldsymbol{J}^{\mathrm{a}}_{\mathrm{S}3z}{}^2 + \boldsymbol{J}^{\mathrm{l}}_{\mathrm{U}3x}{}^2 + \\ \boldsymbol{J}^{\mathrm{l}}_{\mathrm{U}3y}{}^2 + \boldsymbol{J}^{\mathrm{l}}_{\mathrm{U}3z}{}^2 - \boldsymbol{J}_{\mathrm{P1l}}{}^2. \end{cases} \tag{8}$$

Above two equations are about $\boldsymbol{J}_{\mathrm{U1}\alpha}$ and $\boldsymbol{J}_{\mathrm{U1}\beta}$. Solving these equations can obtain these two angles. Then we can use pose matrix ${}^{\mathrm{l}}\boldsymbol{T}_{\mathrm{a}}$ to obtain the foot tip position in the leg coordinate frame C_{l},

$$P^{\mathrm{l}}_{\mathrm{f}} = {}^{\mathrm{l}}\boldsymbol{T}_{\mathrm{a}} \bullet \begin{pmatrix} J^{\mathrm{a}}_{\mathrm{Pfx}} \\ J^{\mathrm{a}}_{\mathrm{Pfy}} \\ J^{\mathrm{a}}_{\mathrm{Pfz}} \\ 1 \end{pmatrix}. \tag{9}$$

Then the inverse kinematics model will be described. On the contrary to the direct kinematics model, the foot tip position $P^{\mathrm{l}}_{\mathrm{f}}$ becomes the input of the model when J_{P1l}, J_{P2l} and J_{P2l} become the output of the model. According to Eq. (1) and Eq. (9), we have

$$\begin{cases} (J_{\mathrm{P1l}} + P^{\mathrm{a}}_{\mathrm{fx}})\cos J_{\mathrm{U1}\alpha} \cos J_{\mathrm{U1}\beta} - P^{\mathrm{a}}_{\mathrm{fy}} \cos J_{\mathrm{U1}\alpha} \sin J_{\mathrm{U1}\beta} + \\ \quad P^{\mathrm{a}}_{\mathrm{fz}} \sin J_{\mathrm{U1a}} = P^{\mathrm{l}}_{\mathrm{fx}}, \\ (J_{\mathrm{P1l}} + P^{\mathrm{a}}_{\mathrm{fx}})\sin J_{\mathrm{U1}\beta} + P^{\mathrm{a}}_{\mathrm{fy}} \cos J_{\mathrm{U1}\beta} = P^{\mathrm{l}}_{\mathrm{fy}}, \\ (J_{\mathrm{P1l}} + P^{\mathrm{a}}_{\mathrm{fx}})\sin J_{\mathrm{U1}\alpha} \cos J_{\mathrm{U1}\beta} - P^{\mathrm{a}}_{\mathrm{fy}} \sin J_{\mathrm{U1}\alpha} \sin J_{\mathrm{U1}\beta} + \\ \quad P^{\mathrm{a}}_{\mathrm{fz}} \cos J_{\mathrm{U1}\alpha} = P^{\mathrm{l}}_{\mathrm{fz}}. \end{cases} \tag{10}$$

Solving Eqs. (10), we will get J_{P1l}, $J_{\mathrm{U1}\alpha}$ and $J_{\mathrm{U1}\beta}$, thus the pose matrix ${}^{\mathrm{l}}\boldsymbol{T}_{\mathrm{a}}$ can be obtained.

Thus, the coordinates of $\boldsymbol{J}_{\mathrm{S2}}$ and $\boldsymbol{J}_{\mathrm{S3}}$ in the coordinate frame C_l can be derived:

$$\begin{cases} \boldsymbol{J}^{\mathrm{l}}_{\mathrm{S2}} = {}^{\mathrm{l}}\boldsymbol{T}_{\mathrm{a}} \bullet \boldsymbol{J}^{\mathrm{a}}_{\mathrm{S2}}, \\ \boldsymbol{J}^{\mathrm{l}}_{\mathrm{S3}} = {}^{\mathrm{l}}\boldsymbol{T}_{\mathrm{a}} \bullet \boldsymbol{J}^{\mathrm{a}}_{\mathrm{S3}}. \end{cases} \tag{11}$$

And, we have

$$\begin{cases} J_{\mathrm{P2l}} = \left| \boldsymbol{J}^{\mathrm{l}}_{\mathrm{S2}} - \boldsymbol{J}^{\mathrm{l}}_{\mathrm{U2}} \right|, \\ J_{\mathrm{P3l}} = \left| \boldsymbol{J}^{\mathrm{l}}_{\mathrm{S3}} - \boldsymbol{J}^{\mathrm{l}}_{\mathrm{U3}} \right|. \end{cases} \tag{12}$$

Thus three displacements of the prismatic joints are calculated from the foot tip position.

3.3 Force estimation model

In the previous subsection, the kinematics models describing the relationship between the motor output position and the foot tip position are established. Having this model is a prerequisite to establish the force Jacobian matrix.

The input and output forces involved in the estimation model are illustrated in Fig. 5. As the shape of the foot is a half sphere, here we assume that the foot tip force is a pure force without torque. This force is denoted as $\boldsymbol{F}_{\mathrm{f}}$, and it has three components F_{fx}, F_{fy} and F_{fz}. Forces generated by the motors' output torque are denoted as $\boldsymbol{F}_{\mathrm{P1}}$, $\boldsymbol{F}_{\mathrm{P2}}$ and $\boldsymbol{F}_{\mathrm{P3}}$. The mapping between these forces is described by a single leg force Jacobian matrix. Yang[25] introduced the derivation of the single leg force Jacobian of the robot's leg mechanism. Then the foot tip force can be calculated by following equation:

$$\begin{pmatrix} F_{\mathrm{fx}} \\ F_{\mathrm{fy}} \\ F_{\mathrm{fz}} \end{pmatrix} = \boldsymbol{J} \times \begin{pmatrix} F_{\mathrm{P1}} \\ F_{\mathrm{P2}} \\ F_{\mathrm{P3}} \end{pmatrix}. \tag{13}$$

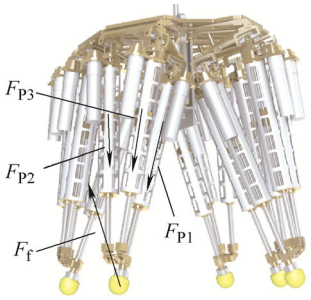

Fig. 5. Forces on one leg of the robot

The basic idea of the derivation of this Jacobian matrix is establishing equilibrium equations of the forces applied on the prismatic joints and the forces exerted on the foot tip. The force equilibrium equation on $\boldsymbol{J}_{\mathrm{P1}}$ direction is

$$\boldsymbol{J}_{\mathrm{P1}} \Big/ \left| \boldsymbol{J}_{\mathrm{P1}} \right| \bullet (\boldsymbol{F}_{\mathrm{P1}} + \boldsymbol{F}_{\mathrm{P2}} + \boldsymbol{F}_{\mathrm{P3}} + \boldsymbol{F}_{\mathrm{f}}) = 0. \tag{14}$$

And, the torque equilibrium equations are

$$\begin{cases} \boldsymbol{A}_{\mathrm{i}} \bullet (\boldsymbol{J}^{\mathrm{l}}_{\mathrm{U1}} \times \boldsymbol{F}_{\mathrm{P1}} + \boldsymbol{J}^{\mathrm{l}}_{\mathrm{U2}} \times \boldsymbol{F}_{\mathrm{P2}} + \boldsymbol{J}^{\mathrm{l}}_{\mathrm{U3}} \times \boldsymbol{F}_{\mathrm{P3}} + \boldsymbol{P}^{\mathrm{l}}_{\mathrm{f}} \times \boldsymbol{F}_{\mathrm{f}}) = 0, \\ \boldsymbol{A}_{\mathrm{j}} \bullet (\boldsymbol{J}^{\mathrm{l}}_{\mathrm{U1}} \times \boldsymbol{F}_{\mathrm{P1}} + \boldsymbol{J}^{\mathrm{l}}_{\mathrm{U2}} \times \boldsymbol{F}_{\mathrm{P2}} + \boldsymbol{J}^{\mathrm{l}}_{\mathrm{U3}} \times \boldsymbol{F}_{\mathrm{P3}} + \boldsymbol{P}^{\mathrm{l}}_{\mathrm{f}} \times \boldsymbol{F}_{\mathrm{f}}) = 0. \end{cases} \tag{15}$$

where $\boldsymbol{A}_{\mathrm{i}}$, $\boldsymbol{A}_{\mathrm{j}}$—Unit vectors of two axis of universal joint $\boldsymbol{J}_{\mathrm{U1}}$.

Expending and rearranging Eqs. (14) and (15), we can get

$$\boldsymbol{J}_2 \times \begin{pmatrix} F_{\mathrm{fx}} \\ F_{\mathrm{fy}} \\ F_{\mathrm{fz}} \end{pmatrix} = \boldsymbol{J}_1 \times \begin{pmatrix} F_{\mathrm{P1}} \\ F_{\mathrm{P2}} \\ F_{\mathrm{P3}} \end{pmatrix}. \tag{16}$$

Thus, we have

$$\boldsymbol{J} = \boldsymbol{J}_2^{-1} \times \boldsymbol{J}_1. \tag{17}$$

4 Method for Stepping on Obstacle

In order to step on the obstacle, the robot needs to negotiate with the environment by applying a kind of adaptive gait. In the previous section, the indirect force estimation model has been established. In this section, based on this model, an adaptive gait is described.

4.1 Forces and motor current

It is sensible to assume that the motor's output torque is in proportion to the motor current. Eq. (18) describes the relationship of the motor current and the motor output torque:

$$T_{\mathrm{m}} = K_{\mathrm{t}} \times I_{\mathrm{m}}, \tag{18}$$

where T_{m} —Motor output torque,
K_{t} —Motor torque constant,
I_{m} —Motor current.

The relationship of force on the crew and motor torque is also can be treated as a linear relationship. It is described by Eq. (19):

$$F_{\mathrm{s}} = \frac{\eta \times T_{\mathrm{m}} \times 2\pi}{S_{\mathrm{l}}}, \tag{19}$$

where F_{s} —Force on the screw,
S_{l} —Lead of the screw,
η —Ball screw efficiency.

The control system of the robot can read motor's current data in every real-time control loop. While the robot is running, the motor output torque, the load torque and dynamic torque form an equilibrium, as described in Eq. (20):

$$T_{\mathrm{m}} = T_{\mathrm{ld}} + T_{\mathrm{dyn}}, \tag{20}$$

where T_{m} —Motor output torque,
T_{ld} —Load torque,
T_{dyn} —Dynamic torque.

$$\begin{cases} T_{\mathrm{ld}} = T_{\mathrm{g}} + T_{\mathrm{e}}, \\ T_{\mathrm{dyn}} = T_{\mathrm{i}} + T_{\mathrm{fr}}, \end{cases} \tag{21}$$

where T_{g} —Torque caused by the gravity,
T_{e} —Torque caused by the external force,
T_{i} —Torque caused by inertial,
T_{fr} —Torque caused by friction.

Now the components of the load torque and the dynamic will be discussed. The load torque includes the torque caused by the constant load, for example, the gravity force exerted on the robot. The dynamic load includes the torque caused in a .transient change. For example, the dynamic torque can be introduced by the acceleration and the deceleration when the leg swings. Eq. (21) describes the load torque and the dynamic torque involved in the robot motion. The idea of the indirect force estimation is finding the relationship between the external forces and the motor output torque. Observing all the torque components, T_{g} always exists, while T_{e} only exists when an external force is applied on the robot. In the experiment condition of this study, only the robot leg will contact with the ground and obstacle. Under such condition T_{e} will appear. The inertial torque will appear when the robot part experiences acceleration and deceleration. As the motor connects to the ball screw, the inertial torque caused by the motion change of the robot part will be reduced. Meanwhile, the inertial torque raised by the rotor of the motor must be taken into consideration; the torque generated by it can be calculated and then be taken out of the motor torque calculated from the current. The friction force mainly exists in the ball screw. This force is assumed to be proportion to the speed of the ball screw. Thus, low speed can lower the torque caused by it.

When the robot is walking in the static gait, there are two states of the leg, the swing state and the support state. In the swing state, there is no external force if there is no obstacle. So in the walking direction the forces calculated from the proposed method are mainly the inertial forces caused by the leg mechanism and the leg gravity. When the leg contacts the obstacle, a change in the calculated force will appear. Then the obstacle is detected. The same thing happened when the foot tip contacts with the ground. In the supporting state, the whole robot's weight is balanced by T_{e}. The parallel leg mechanism of the robot causes big difference between the body weight and the leg weight. These make it reasonable to detect the contact by the indirect force estimation model.

4.2 Adaptive gait

If the robot knows when the leg contacts the ground and the obstacle, the control system can adjust the trajectory of the foot tip to adapt them. Here an adaptive gait is designed based on the design of the robot Octopus III. The robot is designed to pass the uneven terrain and carry heavy load. As a result, its walking velocity is not very high. The static walking is an appropriate choice for this robot. Because the static walking requires the robot being stable all the time, and the robot legs is divided into two groups.

In Fig. 6, different number is assigned to each leg of the robot. The legs 1, 3, 5 form a group, and the left form the other group. In all time the robot has at least three legs contacting with the ground, and these three legs are not on the same side of the body. The center of the mass will lie in the support polygon all the time.

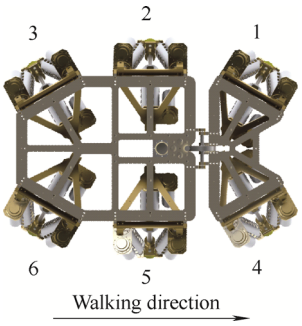

Fig. 6. Numbering the leg

To each single leg, the trajectory is consists of several pieces of straight lines. Fig. 7 illustrates the trajectories of the adaptive gait of one single leg. In situation A, the trajectory is rectangular. The process is consists of moving up, moving forward and moving down. When the leg is moving down, it will use the indirect force estimation to calculate the force along the *y*-axis of the body coordinate frame. If the force is big enough, then the motion will stop. At this time, the foot tip should contact with the ground and support the body. To be clear, as the robot doesn't have an IMU, the motion will assume that the body is in an equilibrium position at the beginning. Situation B is more complex. When the leg is moving forward, the control system will monitor the force along the z-axis of the body coordinate frame. If the force is big enough, the control system will stop the leg from moving forward, and then move the leg backward and up a little. After that, the leg will try to move forward again. Situation C is just like situation B, but it shows that the algorithm will adjust the leg position more than once to enhance the ability to step on the obstacle. In fact the height of the foot tip is limited by the work space of the leg mechanism. All these straight line trajectories are generated according to the given acceleration, deceleration and maximum speed.

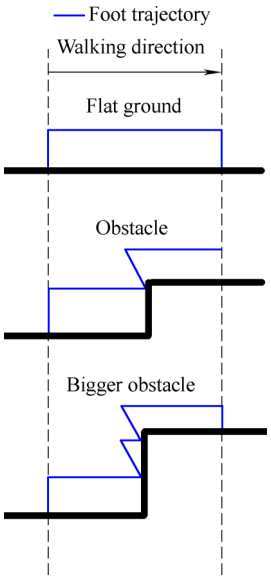

Fig. 7. Adaptive gait of one single leg

Fig. 8 is the flowchart of the adaptive tripod gait. In the experiment, this process is implemented in real time control system. At first, legs 1, 3 and 5 will execute their motion. When these legs are supporting the robot, the body will move forward. Then the other three legs will begin their motion to catch up the first group of legs. Each group of legs will begin their motion together but may not finish their motion at the same time because of the ground and obstacle.

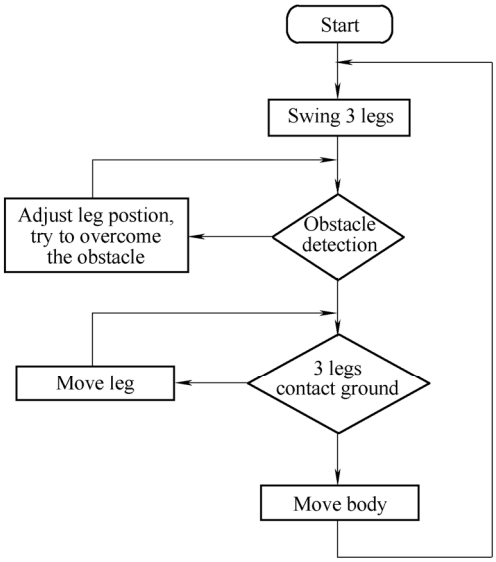

Fig. 8. Flowchart of the adaptive tripod gait

5 Experiments

This section will describe the details and the experiment results of the proposed method.

5.1 External force estimation experiment

The first experiment is designed to validate the proposed indirect force estimation method. Fig. 9 is a photo taken during the experiment.

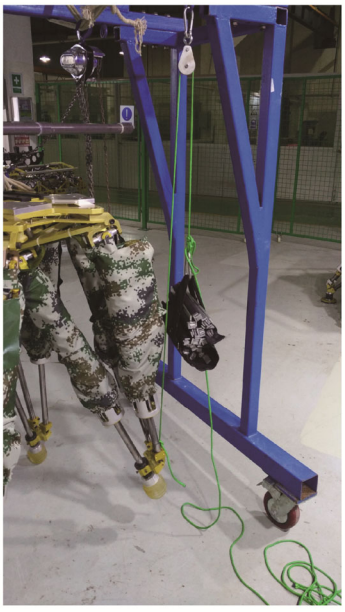

Fig. 9. External force estimate experiment

A pulley was suspended from a fixed beam. Then a string was connect with the one foot tip of the robot, while the other end of the string was connected the load. The string was suspended from the pulley. The load was small iron bars added to the basket gradually. In this experiment, the robot was kept standing still, so the inertia force could be omitted and the gravity did not change during the experiment. The gravity and the external force are two components of the estimated force. Considering the experiment setup, the gravity of the leg was considered as system bias. In order to eliminate this system bias, one set of the experiment data was used as a reference. Then the external force of each load was estimated. Fig. 10 illustrates the relation between the estimated external force and the load applied. It is clear that the estimated forces increase as the load increases. The result demonstrates that the external forces can be estimated by the proposed indirect force estimation method.

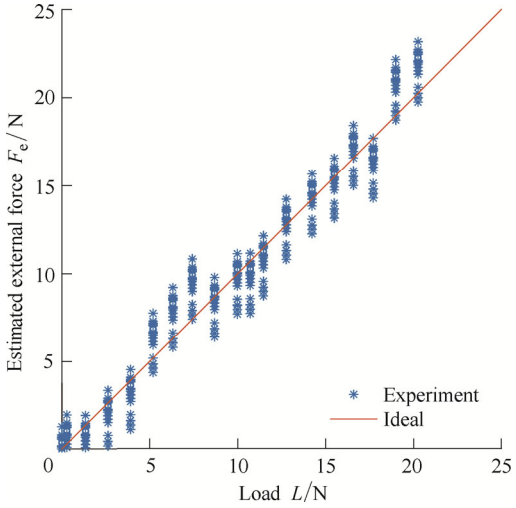

Fig. 10.　Estimated external forces

5.2　Obstacle stepping experiment

Fig. 11 shows the environment of the obstacle stepping experiment. The robot does not have any IMU, so the robot was placed on a flat ground.　In this setting the initial state of the robot was very close to the assumption in the proposed method that the robot started at the equilibrium position. That means y-axis of the robot's body coordinate frame is parallel to the gravity direction. The obstacle consisted of several bricks. Each brick was about 10cm high. So two layers of the bricks are about 20cm high. This experiment was designed to show the robot can step on one layer of bricks and then two layers of the bricks using the proposed method.

Fig. 12 was taken from the second experiment. This fig shows the robot legs 1, 3 and 5 acted like a group. On the flat ground, the rectangular trajectory was used. Each leg stopped after contacting with the ground with certain force.

Fig. 13 shows what happens while the robot met the obstacle. There were obstacles with different height. All the heights were reachable in the leg's workspace. In the experiment, the legs of the right side of the robot stepped on the obstacle gradually. At first only leg 4 was contacted with the obstacle. Then it moved back and up a little to overcome the obstacle. While leg 4 was moving down, the force estimation result was used to detect the foot-ground contact. After that, leg 5 also stepped on the obstacle in the same way. Because the gait changed according to the contact situation during the motion, each leg finished its motion at different time. When the foot on the obstacle was about to start another motion, the algorithm gave a new height of its gait according to both the current position and the workspace. If it contacts with an obstacle, it would adjust its trajectory again. During the experiment, the robot control system didn't modify the posture of the robot body. So the body tended to keep horizontal if there was no disturbance.

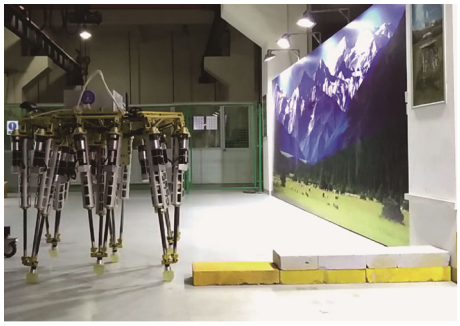

Fig. 11.　Experiment environment

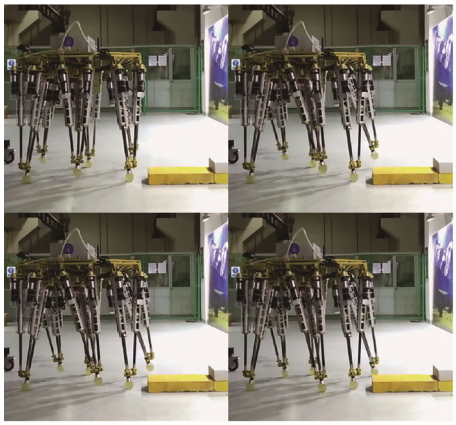

Fig. 12.　Walking pattern of the robot on the flat ground

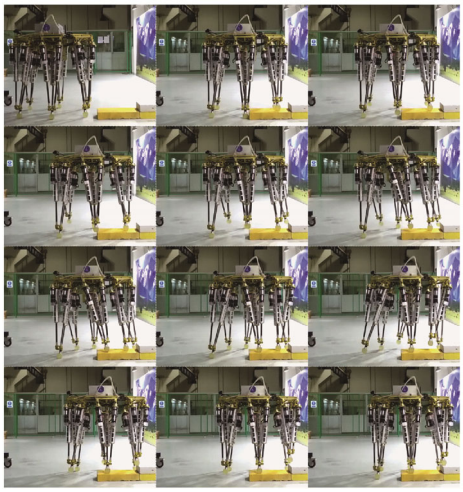

Fig. 13.　Detection and adaption of the obstacle

The data collected from the motor driver are provided here. Fig.14 shows the position of the foot tip of legs 4, 5 and 6 along the *y*-axis of the body coordinate frame. It is clear that the three legs on the right side of the robot gradually stepped on the bricks. Changes of the contact point's height are also illustrated.

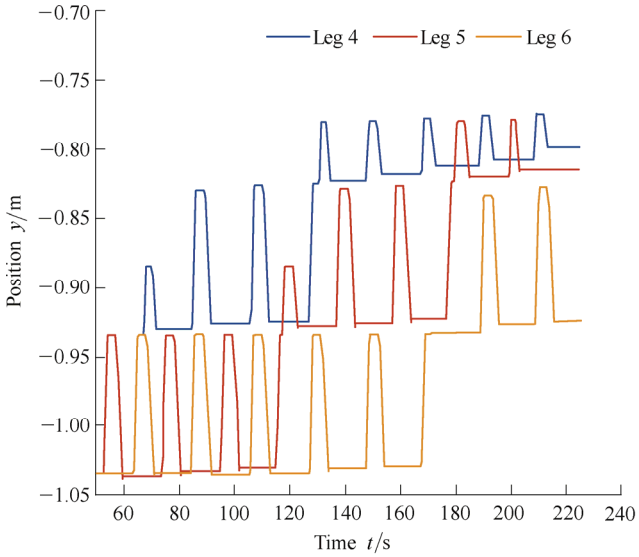

Fig. 14. Foot tip position (along with *y*-axis of the body coordinate frame) in the experiment

Fig. 15 shows the acceleration of the foot tip of legs 4, 5 and 6 along the *y*-axis of the body coordinate frame. The peak on the curve is the point that the body begins to moving forward or finishes moving forward. When the leg is contacting with the ground, the leg will stop at that point. This will also generate a peak on the curve. But when the robot leg is swing forward, the acceleration is relatively small.

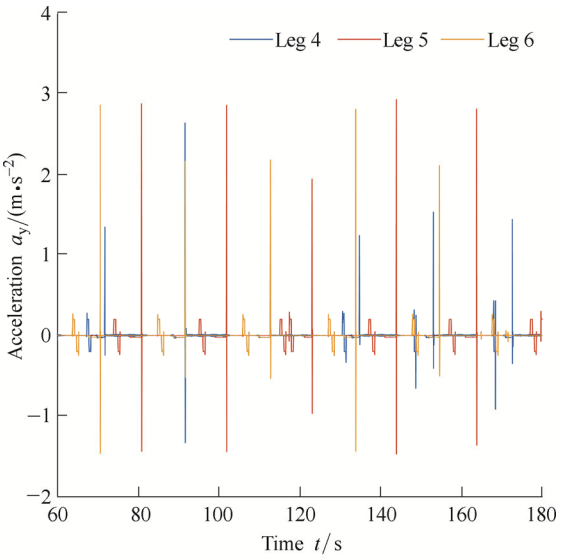

Fig. 15. Foot tip acceleration (along with *y*-axis of the body coordinate frame) in the experiment

Fig. 16 illustrates the current data of three motors (denoted I1, I2 and I3) of leg 5. Although these data do not directly reflect the foot tip forces, we still could find some patterns in the curve.

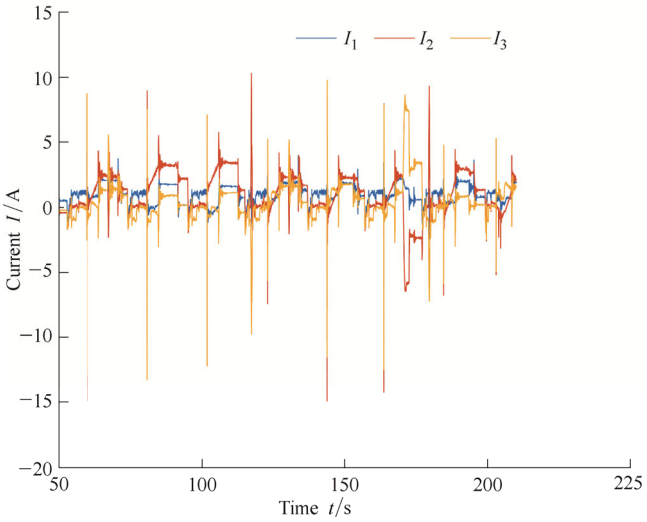

Fig. 16. Current of the three motors in leg 5

Fig. 17 illustrates the foot tip forces of legs 4, 5 and 6 along with the *y*-axis of the body coordinate frame. They were calculated by the indirect force estimation model. According to Fig. 6, leg 5 is on the right side of the robot body and the other two legs are on the other side. The force estimation result agrees with this leg configuration. The estimated force of leg 5 is bigger than that of leg 4 and leg 6.

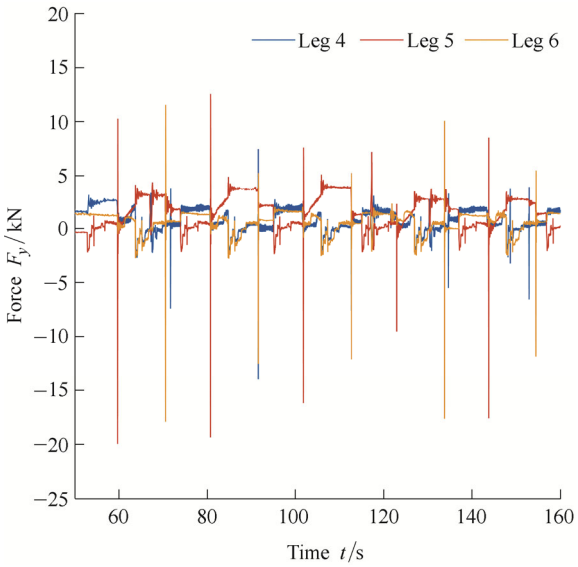

Fig. 17. Estimated foot tip forces (along with *y*-axis of the body coordinate frame)

While the robot leg is moving forward, the leg may stop and adjust its gait. In Fig. 18, the foot tip position along with *z*-axis of the body coordinate frame is illustrated. It is obvious that leg 4 met the obstacle first, and then leg 5.

Fig. 19 shows the acceleration along with *z*-axis of the body coordinate frame. The peak is also caused by sudden change in the gait trajectory, but most of the time the acceleration is relative small. Fig. 20 shows the indirect force estimation result. The three peaks in the graph shows three contact with the obstacle, which means the proposed method is effective in detecting the contact with the

obstacle.

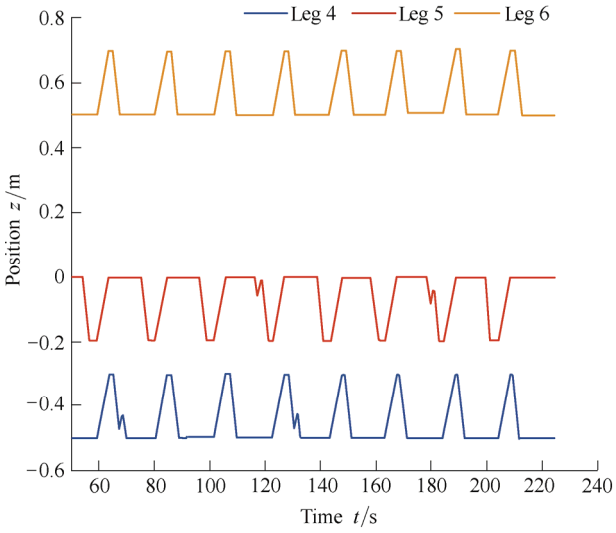

Fig. 18. Foot tip position (along with z-axis of the body coordinate frame)

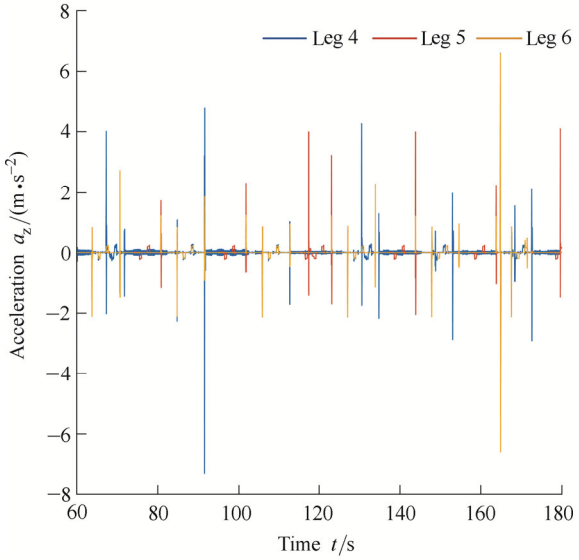

Fig. 19. Foot tip acceleration (along with z-axis of the body coordinate frame)

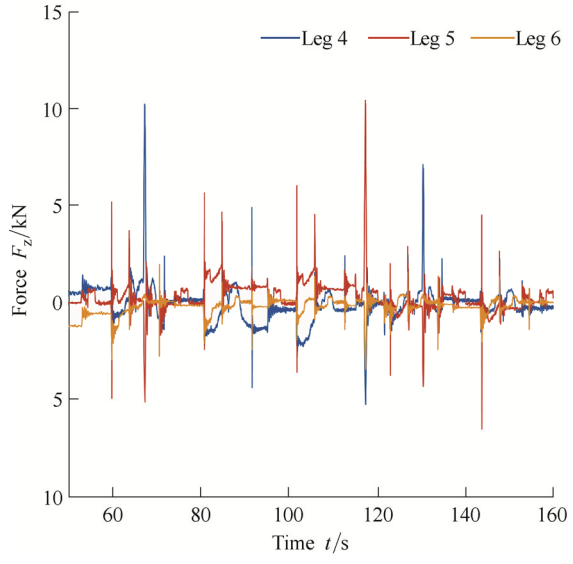

Fig. 20. Estimated foot tip forces (along with z-axis of the body coordinate frame)

6 Conclusions

(1) An indirect force estimation method is established with respect to the robot structure. The external force exerted on the robot foot is calculated from the motor current rather than force sensors.

(2) An adaptive gait is designed based on the proposed indirect force estimation method. The trajectory of the static tripod gait can be modified by the control algorithm according to the changes of contact force.

(3) All the models and algorithm are implemented in the real-time control system of the robot. Experiments are carried out to validate the proposed model and algorithm. The results indicate that the method is effective in detecting contact with the ground or obstacles. The 20 cm height obstacle is stepped on by the robot running the proposed algorithm.

References

[1] CHEN W, REN G, WANG J, et al. An adaptive locomotion controller for a hexapod robot: CPG, kinematics and force feedback[J]. *Science China Information Sciences*, 2014, 57(11): 1–18.

[2] AMARAL P F S, PINTO B G M. A four legged walking robot with obstacle overcoming capabilities[C]//*2010 3rd Conference on Human System Interactions(HSI),* Rzeszow, May 13–15, 2010: 374–379.

[3] HUANG Q-J, NONAMI K. Humanitarian mine detecting six-legged walking robot and hybrid neuro walking control with position/force control[J]. *Mechatronics*, 2003, 13(8): 773–790.

[4] RAIBERT M, BLANKESPOOR K, NELSON G, et al. Bigdog, the rough-terrain quadruped robot[C]//*Proceedings of the 17th World Congress*, The International Federation of Automatic Control, Seoul Korea, July 6–11, 2008 , 17(1): 10822–10825.

[5] SEMINI C, TSAGARAKIS N G, GUGLIELMINO E, et al. Design of HyQ — a hydraulically and electrically actuated quadruped robot[J]. *Proceedings of the Institution of Mechanical Engineers, Part I: Journal of Systems and Control Engineering*, 2011, 225(6): 831–849.

[6] GORINEVSKY D M, SHNEIDER A Y. Force control in locomotion of legged vehicles over rigid and soft surfaces[J]. *The International Journal of Robotics Research*, 1990, 9(2): 4–23.

[7] PRATT J, KRUPP B, MORSE C. Series elastic actuators for high fidelity force control[J]. *Industrial Robot: An International Journal*, 2002, 29(3): 234–241.

[8] DE LUCA A, MATTONE R. Sensorless robot collision detection and hybrid force/motion control[C]//*Proceedings of the 2005 IEEE International Conference on Robotics and Automation, 2005. ICRA 2005*. Barcelona, Spain, April 18–22, 2005: 999–1004.

[9] KATSURA S, MATSUMOTO Y, OHNISHI K. Modeling of force sensing and validation of disturbance observer for force control[J]. *IEEE Transactions on Industrial Electronics*, 2007, 54(1): 530–538.

[10] VASSILEVA D, KIYOSAWA Y, SUZUKI M. Sensorless torque control for a robot with harmonic drive reducers[J]. *Mechanics Based Design of Structures and Machines*, 2011, 39(2): 253–267.

[11] BELLACCINI M, LANARI L, PAOLILLO A, et al. Manual guidance of humanoid robots without force sensors: Preliminary experiments with NAO[C]//*2014 IEEE International Conference on Robotics and Automation(ICRA),* Hong Kong, China, May 31–June 7, 2014: 1184–1189.

[12] OTA Y, YONEDA K, ITO F, et al. Design and control of 6-DOF mechanism for twin-frame mobile robot[J]. *Autonomous Robots*,

2001, 10(3): 297–316.

[13] BACHEGA R P, PIRES R, CAMPO A B. Hardware configuration of hexapod robot to force feedback control development[C]//*2012 44th Southeastern Symposium on System Theory(SSST)*. Jacksonville, Finland, March 11–13, 2012: 115–120.

[14] TIAN X, GAO F, QI C, et al. External disturbance identification of a quadruped robot with parallel-serial leg structure[J]. *International Journal of Mechanics and Materials in Design*, 2014: 1–12.

[15] NABULSI S, SARRIA J F, MONTES H, et al. High-resolution indirect feet-ground interaction measurement for hydraulic-legged robots[J]. *IEEE Transactions on Instrumentation and Measurement*, 2009, 58(10): 3396–3404.

[16] ALBARRAL J L, CELAYA E. Implementation of a driver level with odometry for the LAURON III hexapod robot[M]//*Climbing and Walking Robots*. Springer Berlin Heidelberg, 2005: 135–141.

[17] BOMBLED Q, VERLINDEN O. Current sensing in a six-legged robot[C]//*IUTAM Symposium on Dynamics Modeling and Interaction Control in Virtual and Real Environments*. Budapest, Hungary, June 7–11, 2010: 73–80.

[18] BOMBLED Q, VERLINDEN O. Dynamic simulation of six-legged robots with a focus on joint friction[J]. *Multibody System Dynamics*, 2012, 28(4): 395–417.

[19] SEOK S, WANG A, CHUAH M Y, et al. Design principles for highly efficient quadrupeds and implementation on the MIT Cheetah robot[C]//*2013 IEEE International Conference on Robotics and Automation(ICRA)*. Karlsruhe, Germany, May 6–10, 2013: 3307–3312.

[20] SEOK S, WANG A, OTTEN D, et al. Actuator design for high force proprioceptive control in fast legged locomotion[C]// *2012 IEEE/RSJ International Conference on Intelligent Robots and Systems(IROS),* Vilamoura, Algarve, Portugal, October 7–12, 2012: 1970–1975.

[21] WU J, LI T, XU B. Force optimization of planar 2-DOF parallel manipulators with actuation redundancy considering deformation[J]. *Proceedings of the Institution of Mechanical Engineers, Part C: Journal of Mechanical Engineering Science*, 2012: 1371–1377.

[22] WU J, WANG D, WANG L. A control strategy of a 2-DOF heavy duty parallel manipulator[J]. *Journal of Dynamic Systems, Measurement, and Control*, 2014, 137(6): 061007-1–061007-10

[23] WU J, WANG J, WANG L, et al. Dynamics and control of a planar 3-DOF parallel manipulator with actuation redundancy[J]. *Mechanism and Machine Theory*, 2009, 44(4): 835–849.

[24] PAN Y, GAO F. A new 6-parallel-legged walking robot for drilling holes on the fuselage[J]. *Proceedings of the Institution of Mechanical Engineers, Part C: Journal of Mechanical Engineering Science*, 2013, 228(4): 753–764.

[25] PAN Y, GAO F. Leg kinematic analysis and prototype experiments of walking-operating multifunctional hexapod robot[J]. *Proceedings of the Institution of Mechanical Engineers, Part C: Journal of Mechanical Engineering Science*, 2014, 228(12): 2217–2232.

[26] HUANG T, LI M, ZHAO X, et al. Conceptual design and dimensional synthesis for a 3-DOF module of the TriVariant-a novel 5-DOF reconfigurable hybrid robot[J]. *IEEE Transactions on Robotics*, 2005, 21(3): 449–456.

Biographical notes

XU Yilin, born in 1989, is currently a PhD candidate at *State Key Laboratory of Mechanical System and Vibration, Shanghai Jiao Tong University, China*. His research interests include control of the legged robots.
E-mail: xuyilin@sjtu.edu.cn

GAO Feng, born in 1956, is currently a professor at *State Key Laboratory of Mechanical System and Vibration, Shanghai Jiao Tong University, China*. His main research interests include parallel robots, design theory and its applications, large scale and heavy payload manipulator design, large scale press machine design and optimization, design and manufactory of nuclear power equipment, legged robots design and control.
E-mail: fengg@sjtu.edu.cn

PAN Yang, born in 1988, is currently a post-doctor at *State Key Laboratory of Mechanical System and Vibration, Shanghai Jiao Tong University, China*. His research interests include design and control of legged robots.
E-mail: py0330@sjtu.edu.cn

CHAI Xun, born in 1990, is currently a PhD candidate at *State Key Laboratory of Mechanical System and Vibration, Shanghai Jiao Tong University, China.* His research interest is visual control of legged robots.
E-mail: chaixun@sjtu.edu.cn